



# An alumina-supported silver catalyst with high water tolerance for H<sub>2</sub> assisted C<sub>3</sub>H<sub>6</sub>-SCR of NO<sub>x</sub>



Guangyan Xu<sup>a,b,1</sup>, Jinzhu Ma<sup>a,b,c,1</sup>, Guangzhi He<sup>a</sup>, Yunbo Yu<sup>a,b,c,\*</sup>, Hong He<sup>a,b,c,\*</sup>

<sup>a</sup> State key Joint Laboratory of Environment Simulation and Pollution Control, Research Center for Eco-Environmental Sciences, Chinese Academy of Sciences, Beijing 100085, China

<sup>b</sup> University of Chinese Academy of Sciences, Beijing 100049, China

<sup>c</sup> Center for Excellence in Regional Atmospheric Environment, Institute of Urban Environment, Chinese Academy of Sciences, Xiamen 361021, China

## ARTICLE INFO

### Article history:

Received 11 November 2016

Received in revised form 20 January 2017

Accepted 1 February 2017

Available online 1 February 2017

### Keywords:

Ag/Al<sub>2</sub>O<sub>3</sub>

HC-SCR

Water vapor

H<sub>2</sub>

DFT

## ABSTRACT

Water vapor is typically present in diesel engine exhausts, and thus the design of catalysts with high water-tolerance is highly desired. The addition of water vapor was shown to have quite different influences on the activity of Ag/Al<sub>2</sub>O<sub>3</sub> catalysts with different Ag loadings during the H<sub>2</sub>-assisted C<sub>3</sub>H<sub>6</sub>-SCR of NO<sub>x</sub> (H<sub>2</sub>-C<sub>3</sub>H<sub>6</sub>-SCR). The 2 wt% Ag/Al<sub>2</sub>O<sub>3</sub> catalyst showed the best activity for H<sub>2</sub>-C<sub>3</sub>H<sub>6</sub>-SCR, with excellent water resistance over the whole temperature range. An enhancement in NO<sub>x</sub> conversion was observed after water vapor was introduced, particularly at low temperatures. Over this catalyst, kinetic studies confirmed that H<sub>2</sub>O addition did not change the apparent activation energy for NO<sub>x</sub> reduction, while it increased the reaction order of C<sub>3</sub>H<sub>6</sub> from −0.62 to 0.73. This result indicated that the reaction pathway for NO<sub>x</sub> reduction was hardly changed by the introduction of water vapor, while a poisoning effect related to C<sub>3</sub>H<sub>6</sub> oxidation was decreased. *In situ* DRIFTS studies and DFT calculations revealed that water vapor significantly inhibits the formation of inert formate during the H<sub>2</sub>-C<sub>3</sub>H<sub>6</sub>-SCR process, and thus more sites are available for the formation of active enolic species and acetates, finally leading to increased activity for 2 wt% Ag/Al<sub>2</sub>O<sub>3</sub> in NO<sub>x</sub> reduction.

© 2017 Elsevier B.V. All rights reserved.

## 1. Introduction

Nitrogen oxides (NO<sub>x</sub>), as key precursors to pollutants, induce the formation of acid rain, photochemical smog, and haze. Nowadays, diesel engine NO<sub>x</sub> after-treatment is one of the greatest challenges in environmental protection. To this aim, different technologies have been developed, among which selective catalytic reduction by hydrocarbons (HC-SCR) has been paid much attention in the past few decades, considering that the on-board diesel or a fuel additive can be used as the reducing agent for NO<sub>x</sub> removal, thus providing an opportunity for simplification of the after-treatment system [1–4]. Previous studies have proved that Ag/Al<sub>2</sub>O<sub>3</sub> is one of the most promising catalysts for NO<sub>x</sub> reduction by hydrocarbons [1–3,5–10]. At low temperatures, however, the activity of Ag/Al<sub>2</sub>O<sub>3</sub> for HC-SCR is not sufficient for its commercial usage in purification of diesel vehicle exhausts.

\* Corresponding authors at: State key Joint Laboratory of Environment Simulation and Pollution Control, Research Center for Eco-Environmental Sciences, Chinese Academy of Sciences, Beijing 100085, China.

E-mail addresses: [ybyu@rcees.ac.cn](mailto:ybyu@rcees.ac.cn) (Y. Yu), [honghe@rcees.ac.cn](mailto:honghe@rcees.ac.cn) (H. He).

<sup>1</sup> These authors contributed equally.

The discovery of a promoting effect of hydrogen on the low-temperature activity of Ag/Al<sub>2</sub>O<sub>3</sub> catalysts by Satokawa et al. [11,12] is undoubtedly a major breakthrough for HC-SCR. Since then, many efforts have been devoted to understanding the “H<sub>2</sub> effect” occurring during NO<sub>x</sub> reduction by lighter hydrocarbons [13–17], higher hydrocarbons [18,19] and alcohols [20] over silver catalysts. At present, the origin of H<sub>2</sub> boosting behavior on the low-temperature activity of Ag/Al<sub>2</sub>O<sub>3</sub> for NO<sub>x</sub> reduction by hydrocarbons has not been revealed in full detail, while it is clear that the presence of H<sub>2</sub> enhances the transformation of hydrocarbons to partially oxidized species. These oxygenates have been proved to be active intermediates for NO<sub>x</sub> reduction, leading to an increase in the NO<sub>x</sub> conversion at low temperatures [15,21–23].

Water vapor is inevitably present in diesel engine exhausts and thus the design of catalysts with high water tolerance is highly desired. However, the influence of water vapor on HC-SCR processes has attracted a limited number of investigations [24–26]. The water tolerance of the 2 wt% Ag/Al<sub>2</sub>O<sub>3</sub> catalyst for NO<sub>x</sub> reduction by different alkanes was studied by Shimizu et al. [24]. It was found that the activity of Ag/Al<sub>2</sub>O<sub>3</sub> for NO<sub>x</sub> reduction and its water resistance were gradually increased with an increase in the carbon number of alkanes. In the case of *n*-octane as a reductant, a signif-

icant promotion effect on NO<sub>x</sub> conversion was induced by water vapor addition, the occurrence of which possibly related to an inhibition of the unselective oxidation of *n*-octane and a suppression of poisoning by carboxylate and carbonate species. Over 1.2 wt% Ag/Al<sub>2</sub>O<sub>3</sub>, a significant loss in NO<sub>x</sub> conversion induced by the presence of H<sub>2</sub>O was observed by Meunier et al. [25] during C<sub>3</sub>H<sub>6</sub>-SCR. As for C<sub>3</sub>H<sub>8</sub>-SCR and H<sub>2</sub>-C<sub>3</sub>H<sub>8</sub>-SCR over 5 wt% Ag/Al<sub>2</sub>O<sub>3</sub>, decreased NO<sub>x</sub> conversion was also observed in the presence of water vapor [27].

It is well-known that silver loading has a great influence on the activity of Ag/Al<sub>2</sub>O<sub>3</sub> catalysts for NO<sub>x</sub> reduction by hydrocarbons [28–30], and also for H<sub>2</sub>-assisted HC-SCR processes [31–33]. To the best of our knowledge, however, there has been no study focusing on the effect of silver loading on the water tolerance of Ag/Al<sub>2</sub>O<sub>3</sub> for H<sub>2</sub>-assisted HC-SCR. Herein, it was found that silver loading governs the water tolerance of Ag/Al<sub>2</sub>O<sub>3</sub> for H<sub>2</sub>-C<sub>3</sub>H<sub>6</sub>-SCR. Based on a kinetic study and *in situ* DRIFTS measurements, the origin of the water vapor effect on the pathway of H<sub>2</sub>-C<sub>3</sub>H<sub>6</sub>-SCR was revealed. This investigation could offer new insights into the design of silver catalysts for HC-SCR with high water resistance.

## 2. Materials and methods

### 2.1. Catalyst preparation and characterization

A series of Ag/Al<sub>2</sub>O<sub>3</sub> catalysts with varying Ag loadings (1, 2, 4, and 6 wt%) were synthesized by an impregnation method, with boehmite (SASOL, SB-1) and silver nitrate as the precursors. The detailed information can be found in our previous studies [2,34]. All the samples presented here were calcined in air at 600 °C for 3 h. A pure Al<sub>2</sub>O<sub>3</sub> sample was also prepared by the same procedure, with boehmite as the precursor.

The BET surface area measurements were carried out on a Quantachrome Autosorb-1C instrument at –196 °C. X-ray powder diffraction patterns were measured on a Rigaku D/max-RB X-ray Diffractometer (Japan) with Cu K $\alpha$  radiation (over the 2 $\theta$  range from 10° to 80°).

UV-vis spectra were collected with a UV-vis spectrophotometer (Hitachi, U3100, Japan) within a range of 200–800 nm with a resolution of 5 nm, using Al<sub>2</sub>O<sub>3</sub> as reference to confirm the baseline spectrum. XANES analyses of the Ag-K edges were performed in transmission mode at the BL14W1 XAFS beam line at the Shanghai Synchrotron Radiation Facility (SSRF). The PE storage ring was operated at 3.5 GeV with 200 mA as the average storage current. Data were analyzed using the Athena program.

### 2.2. Catalyst activity studies

The catalytic measurements were performed in a fixed-bed reactor, by stepwise increase of the temperature and measurement after 30 min reaction at each temperature [35,36]. The feed composition included 800 ppm NO, 1714 ppm C<sub>3</sub>H<sub>6</sub>, 1% H<sub>2</sub> (if added), 10% O<sub>2</sub>, 10% H<sub>2</sub>O (if added) in N<sub>2</sub> balance at a total flow of 1000 ml/min, corresponding to a gas hourly space velocity (GHSV) of 100,000 h<sup>–1</sup> (ca 0.3 g catalyst). The concentrations of NO, NO<sub>2</sub>, NH<sub>3</sub>, N<sub>2</sub>O, and C<sub>3</sub>H<sub>6</sub> were measured by an FTIR spectrometer (Nicolet Nexus is10). Water vapor was supplied into the gas stream with a micro-pump and further vaporized by an electric heater. To avoid water condensation, the gas-filled tube and the gas cell of the FTIR spectrophotometer were heated to 120 °C. NO<sub>x</sub> conversion and C<sub>3</sub>H<sub>6</sub> conversion were calculated as shown in the following equations, respectively:

$$\text{NO}_x \text{ conversion} = \frac{[\text{NO}]_{in} + [\text{NO}_2]_{in} - [\text{NO}]_{out} - [\text{NO}_2]_{out}}{[\text{NO}]_{in} + [\text{NO}_2]_{in}} \times 100\% \quad (1)$$

$$\text{C}_3\text{H}_6 \text{ conversion} = \frac{[\text{C}_3\text{H}_6]_{in} - [\text{C}_3\text{H}_6]_{out}}{[\text{C}_3\text{H}_6]_{in}} \times 100\% \quad (2)$$

### 2.3. Kinetic studies

The apparent activation energy (E<sub>a</sub>) and reaction order for NO<sub>x</sub> reduction were measured in the fixed-bed reactor as described above. To eliminate both internal diffusion and external mass transfer resistances, corresponding experiments were performed with results shown in Fig. S1 and Supplementary material. Based on these results, samples with a particle size of 0.45–0.9 mm were used for kinetic measurement. The value of GHSV was varied in the range of 100,000–3,000,000 h<sup>–1</sup> in order to keep NO<sub>x</sub> conversion below 20%. Before kinetic measurements, all samples were pretreated in 10% O<sub>2</sub>/N<sub>2</sub> at 450 °C for 30 min.

In agreement with previous studies [35,37], the reaction rate of NO<sub>x</sub> conversion (–R<sub>NO<sub>x</sub></sub>) can be calculated from the kinetic data as follows:

$$-R_{\text{NO}_x} \text{ (mol/m}^2\text{/s)} = F_{\text{NO}_x} \times X_{\text{NO}_x} / (W \times S) \quad (3)$$

where F<sub>NO<sub>x</sub></sub> is the molar flow rate of NO<sub>x</sub> (mol/s), X<sub>NO<sub>x</sub></sub> is the conversion of NO<sub>x</sub>, W is the weight of catalyst, and S is the BET surface area. Based on the above results, the Arrhenius plots for NO<sub>x</sub> reduction under different conditions were drawn, and then the related activation energies were calculated from the slope of the plots.

### 2.4. In situ DRIFTS studies

*In situ* DRIFTS experiments were performed on a Nicolet Nexus FI-IR spectrometer (Nexus 670) with 30 scans at a resolution of 4 cm<sup>–1</sup>, under a total gas flow rate of 300 ml/min. Water vapor (5%) was supplied by passing the gas flow through a water bottle, with the gas line heated to 120 °C to avoid water condensation. Before each measurement, the Ag/Al<sub>2</sub>O<sub>3</sub> catalysts were pretreated in 10% O<sub>2</sub>/N<sub>2</sub> at 350 °C for 0.5 h, which was followed by cooling down to the desired temperature to measure a background spectrum.

### 2.5. DFT calculations

All DFT calculations were carried out by use of the CASTEP package from Accelrys. The Perdew–Wang (PW91) functional of the generalized gradient approximation (GGA) was used as the exchange–correlation function. Convergence tests were done for all initial parameters. The interaction between valence electrons and the ionic core was described by an ultrasoft pseudopotential. The vacuum gap was 20 Å to avoid inter-slab interactions in the periodic systems. Calculations were carried out with a plane-wave energy cutoff of 400 eV. Based on our previous reports [38,39], the dehydrated (100) and (110) surfaces of  $\gamma$ -Al<sub>2</sub>O<sub>3</sub> were modeled using a (2 × 2) supercells and four-layer-thick slabs, Al<sub>80</sub>O<sub>120</sub> with surface area of 11.17 × 16.83 Å<sup>2</sup> and Al<sub>64</sub>O<sub>96</sub> with surface area of 16.83 × 16.14 Å<sup>2</sup>, respectively. For the Ag/Al<sub>2</sub>O<sub>3</sub> (100) surface (Ag–O–Al<sub>octa</sub> entities) and Ag/Al<sub>2</sub>O<sub>3</sub> (110) surface (Ag–O–Al<sub>tetra</sub> entities), the AgO units adsorbed on the Al<sub>2</sub>O<sub>3</sub> surfaces mentioned above were established and relaxed (Fig. S2) [38]. To investigate the effect of H<sub>2</sub>O on the adsorption of the adsorbates, the Ag/Al<sub>2</sub>O<sub>3</sub> surfaces were hydroxylated. The 12OH-Ag/Al<sub>2</sub>O<sub>3</sub> (100) surface and 20OH-Ag/Al<sub>2</sub>O<sub>3</sub> (110) surface were established according to previous calculations [40], and the coverage of hydroxyl was calculated to be 6.4 OH nm<sup>–2</sup> and 7.4 OH nm<sup>–2</sup>, respectively. According to our earlier convergence test, the Monkhorst–Pack k-point sets of (2 × 1 × 1) and (1 × 1 × 1) were used for the Al<sub>2</sub>O<sub>3</sub> (100) and Al<sub>2</sub>O<sub>3</sub> (110) surfaces, respectively [38]. The top two layers and the adsorbents were fully relaxed, while the bottom two layers were fixed to mimic the bulk region. The relaxed structures of the hydroxylated Ag/Al<sub>2</sub>O<sub>3</sub> slabs are shown in Fig. S3.

**Table 1**  
Structure parameters of Ag/Al<sub>2</sub>O<sub>3</sub> catalysts with different silver loadings.

Sample	BET surface area (m <sup>2</sup> /g)	Pore volume (cm <sup>3</sup> /g)	Pore diameter (nm)
γ-Al <sub>2</sub> O <sub>3</sub>	271.2	0.59	10.33
1 wt% Ag/Al <sub>2</sub> O <sub>3</sub>	222.5	0.56	10.13
2 wt% Ag/Al <sub>2</sub> O <sub>3</sub>	220.8	0.55	9.91
4 wt% Ag/Al <sub>2</sub> O <sub>3</sub>	220.6	0.51	9.33
6 wt% Ag/Al <sub>2</sub> O <sub>3</sub>	214.7	0.48	8.99

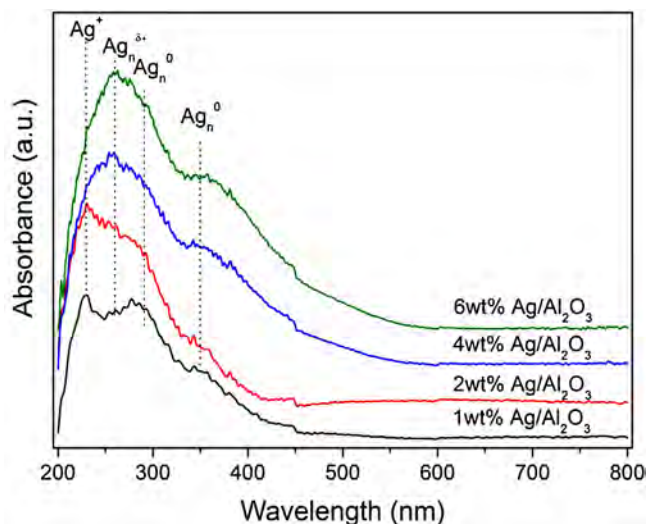


**Fig. 1.** The UV–vis spectra of Ag/Al<sub>2</sub>O<sub>3</sub> catalysts with different silver loadings.

The adsorption energies of the intermediates produced by partial oxidation of C<sub>3</sub>H<sub>6</sub> (HCOO<sup>-</sup>, CH<sub>2</sub>=CHO<sup>-</sup>, and CH<sub>3</sub>COO<sup>-</sup>) on the Ag/Al<sub>2</sub>O<sub>3</sub> surface or the hydroxylated one were calculated as follows:

$$E_{\text{ad}} = E_{\text{adsorbate+surface}} - (E_{\text{surface}} + E_{\text{adsorbate}}),$$

where  $E_{\text{adsorbate+surface}}$  and  $E_{\text{surface}}$  are the total energies of the adsorbed system and alumina slab, respectively; and  $E_{\text{ad}}$  reflects the stability of the adsorbates on either the Ag/Al<sub>2</sub>O<sub>3</sub> or the hydroxylated Ag/Al<sub>2</sub>O<sub>3</sub> surface. Negative  $E_{\text{ad}}$  values mean that the adsorbed state is energetically favorable.

### 3. Results

#### 3.1. Structural properties of Ag/Al<sub>2</sub>O<sub>3</sub> catalysts

As shown in Table 1, the Al<sub>2</sub>O<sub>3</sub> exhibited a BET surface area of 271.2 m<sup>2</sup>/g. Compared with the pure Al<sub>2</sub>O<sub>3</sub>, the Ag/Al<sub>2</sub>O<sub>3</sub> catalysts showed a decrease in surface area, particularly the catalysts with high silver loading [34,35,41]. XRD patterns showed that only the γ-Al<sub>2</sub>O<sub>3</sub> phase was detected in all Ag/Al<sub>2</sub>O<sub>3</sub> catalysts, indicating that Ag was dispersed well on the Al<sub>2</sub>O<sub>3</sub> (Fig. S4).

To investigate the state of silver supported on Al<sub>2</sub>O<sub>3</sub>, UV–vis analysis was performed, with results shown in Fig. 1. According to the literature [4,18,42], the band located at 230 nm is attributed to silver cations (Ag<sup>+</sup>) with high dispersion. The appearance of the peak at 260 nm indicates that oxidized silver clusters (Ag<sub>n</sub><sup>δ+</sup>) are present on the surface of Ag/Al<sub>2</sub>O<sub>3</sub>. In addition, peaks appearing at 290 and 350 nm can be assigned to metallic silver clusters (Ag<sub>n</sub><sup>0</sup>). On the 1 wt% and 2 wt% Ag/Al<sub>2</sub>O<sub>3</sub>, notably, the band at 230 nm exhibited the highest intensity, indicating that highly dispersed silver ions were predominant. As for the samples with 4 wt% and 6 wt% silver loadings, however, the intensity of the band at 260 nm was the highest, suggesting that the silver species were mainly

present as oxidized silver clusters. For these two samples, meanwhile, strong peaks at 350 nm were clearly observed, indicating the existence of numerous metallic silver clusters [2,34,35].

To better understand the precise chemical state of supported silver, the Ag-K XANES spectra of samples with different silver loadings, Ag foil, and AgNO<sub>3</sub> were investigated (Fig. S5). As shown in Fig. S5A, the Ag/Al<sub>2</sub>O<sub>3</sub> catalysts showed Ag-K adsorption edge energies similar to that of AgNO<sub>3</sub>, while being higher than that of Ag foil. The first-order derivative peak for 2 wt%, 4 wt%, 6 wt% Ag/Al<sub>2</sub>O<sub>3</sub> catalysts and AgNO<sub>3</sub> appeared at 25517.5 eV, 25516.4 eV, 25516.7 eV, and 25518.6 eV, respectively. In contrast, the corresponding absorption edge energy for the Ag-K edge in Ag foil was 25514.4 eV (Fig. S5B). These findings further confirm that silver species were mainly present as oxidized silver on 2 wt% Ag/Al<sub>2</sub>O<sub>3</sub>, while the silver species exhibited a partially metallic state on 4 wt% and 6 wt% Ag/Al<sub>2</sub>O<sub>3</sub> [34].

#### 3.2. Effect of H<sub>2</sub>O on the deNO<sub>x</sub> activity of Ag/Al<sub>2</sub>O<sub>3</sub>

Fig. 2 shows that the low-temperature activity of Ag/Al<sub>2</sub>O<sub>3</sub> for C<sub>3</sub>H<sub>6</sub>-SCR can be promoted greatly by H<sub>2</sub> introduction. In the absence of water vapor, it should be noted that the higher the silver loading, the better the low-temperature activity of Ag/Al<sub>2</sub>O<sub>3</sub> for H<sub>2</sub>-assisted C<sub>3</sub>H<sub>6</sub>-SCR (denoted as H<sub>2</sub>-C<sub>3</sub>H<sub>6</sub>-SCR) is. During this H<sub>2</sub>-C<sub>3</sub>H<sub>6</sub>-SCR process, however, water vapor exhibits quite a different influence on NO<sub>x</sub> conversion, which is also closely related to the silver loading. Over 1 wt% Ag/Al<sub>2</sub>O<sub>3</sub>, water vapor had little influence on H<sub>2</sub>-C<sub>3</sub>H<sub>6</sub>-SCR at temperatures below 420 °C, while further increasing the reaction temperature (>420 °C) significantly lowered the NO<sub>x</sub> conversion. In the presence of H<sub>2</sub>, the catalyst with 2 wt% silver loading exhibited excellent activity for NO<sub>x</sub> conversion, achieving 100% NO<sub>x</sub> conversion over a wide temperature range of 295–530 °C. What is more, this catalyst exhibited high water resistance, particularly at low temperatures. Over this sample, indeed, one can easily find an enhancement of NO<sub>x</sub> conversion at temperatures below 300 °C. Compared with 2 wt% Ag/Al<sub>2</sub>O<sub>3</sub>, the samples with silver loadings of 4 wt% and 6 wt% showed better low-temperature activity for NO<sub>x</sub> reduction in the presence of H<sub>2</sub>. However, their activity was severely suppressed by the introduction of water vapor over the whole temperature range. In the presence of water vapor, the 2 wt% Ag/Al<sub>2</sub>O<sub>3</sub> clearly exhibited the highest activity for H<sub>2</sub>-C<sub>3</sub>H<sub>6</sub>-SCR, indicating excellent water resistance.

During the H<sub>2</sub>-C<sub>3</sub>H<sub>6</sub>-SCR process, C<sub>3</sub>H<sub>6</sub> conversion was also measured, with results shown in Fig. 3. At temperatures below 400 °C, the activity of 1 wt% Ag/Al<sub>2</sub>O<sub>3</sub> for C<sub>3</sub>H<sub>6</sub> conversion was hardly changed by water introduction, while at high temperatures, C<sub>3</sub>H<sub>6</sub> conversion obviously decreased with the addition of water vapor. Over the 2 wt% Ag/Al<sub>2</sub>O<sub>3</sub>, the C<sub>3</sub>H<sub>6</sub> conversion at low temperatures was enhanced by the introduction of H<sub>2</sub>O. As for the 4 wt% and 6 wt% Ag/Al<sub>2</sub>O<sub>3</sub> samples, the presence of water vapor severely suppressed C<sub>3</sub>H<sub>6</sub> conversion in the whole temperature range.

Combining the results of Figs. 2 and 3, one can easily find that over a given sample, the changes in NO<sub>x</sub> and C<sub>3</sub>H<sub>6</sub> conversion exhibit the same trend when water vapor is introduced, indicating that C<sub>3</sub>H<sub>6</sub> oxidation plays a crucial role in the reduction of NO<sub>x</sub>. To further confirm such influence of water vapor on H<sub>2</sub>-assisted C<sub>3</sub>H<sub>6</sub>-SCR, a series of step-response experiments were carried out over Ag/Al<sub>2</sub>O<sub>3</sub>, at the temperatures of 265 °C and 400 °C, respectively (Figs. 4 and S6). In these cases, the weight of sample employed was varied in the range of 0.1–0.4 g in order to keep NO<sub>x</sub> conversion below 90%. Over the sample with 2 wt% silver loading, the NO<sub>x</sub> conversion at 265 °C was increased from 22% to 38% by the introduction of water vapor, while it returned to 20% after the removal of water vapor (Fig. 4A). During this process, meanwhile, the C<sub>3</sub>H<sub>6</sub> conversion showed the same trend as the NO<sub>x</sub> conversion, further

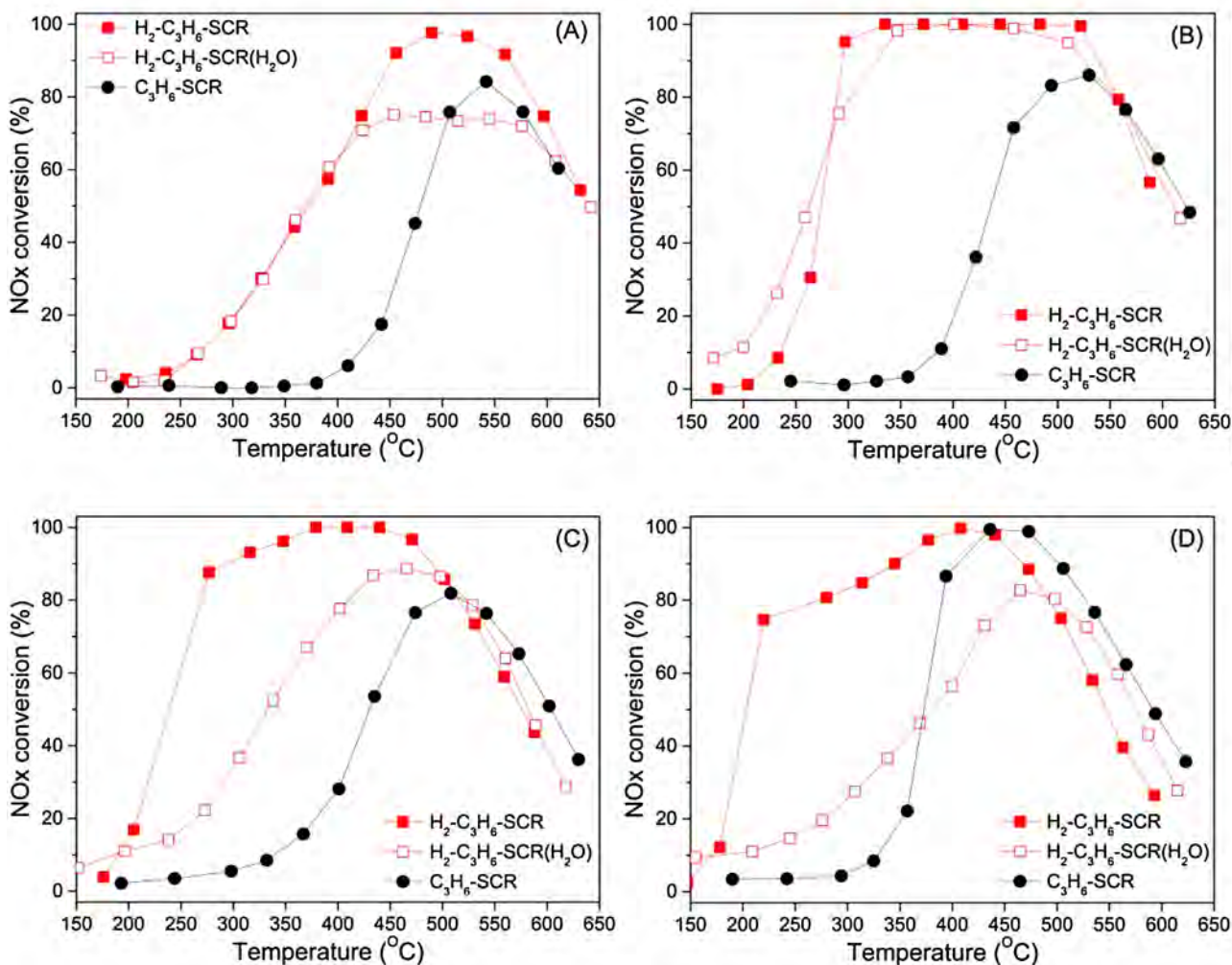


**Fig. 2.** NOx conversions over (A) 1 wt% Ag/Al<sub>2</sub>O<sub>3</sub>, (B) 2 wt% Ag/Al<sub>2</sub>O<sub>3</sub>, (C) 4 wt% Ag/Al<sub>2</sub>O<sub>3</sub>, and (D) 6 wt% Ag/Al<sub>2</sub>O<sub>3</sub> under different conditions: H<sub>2</sub>-C<sub>3</sub>H<sub>6</sub>-SCR (■), H<sub>2</sub>-C<sub>3</sub>H<sub>6</sub>-SCR with H<sub>2</sub>O (□), and C<sub>3</sub>H<sub>6</sub>-SCR (●). Feed composition: 800 ppm NO, 1714 ppm C<sub>3</sub>H<sub>6</sub>, 1% H<sub>2</sub> (when added), 10% H<sub>2</sub>O (when added), 10% O<sub>2</sub>, N<sub>2</sub> balance. GHSV: 100,000 h<sup>-1</sup>.

confirming a crucial role of C<sub>3</sub>H<sub>6</sub> partial oxidation in the reduction of NOx. At the same reaction temperature, however, the activity of 4 wt% Ag/Al<sub>2</sub>O<sub>3</sub> was suppressed severely by water vapor addition (from 74% to 27%), accompanied by a significant loss in C<sub>3</sub>H<sub>6</sub> conversion (Fig. 4B). After the removal of water vapor, again, both the NOx and C<sub>3</sub>H<sub>6</sub> conversion was restored to the original levels. Even at the temperature of 400 °C, the activity of 2 wt% Ag/Al<sub>2</sub>O<sub>3</sub> for NOx and C<sub>3</sub>H<sub>6</sub> conversion was hardly affected by the addition of water vapor (Fig. 4C), further confirming its excellent water tolerance. As shown in Fig. S6, the performance of 1 wt% Ag/Al<sub>2</sub>O<sub>3</sub> for NOx and C<sub>3</sub>H<sub>6</sub> conversion was slightly enhanced by the addition of water vapor, while the low-temperature activity of 6 wt% Ag/Al<sub>2</sub>O<sub>3</sub> was severely suppressed (NOx conversion decreased from 55% to 15%).

### 3.3. Kinetic studies of Ag/Al<sub>2</sub>O<sub>3</sub> for H<sub>2</sub>-C<sub>3</sub>H<sub>6</sub>-SCR

#### 3.3.1. Apparent activation energy

Kinetics has been shown to be extremely valuable in providing unique information on the understanding of catalytic reactions at a molecular level [43], and much attention has been paid to the kinetics of HC-SCR processes [13,24,27,29,31,35,37,41,44–55]. With this in mind, we also carried out kinetic experiments to gain further insights into the influence of water vapor in H<sub>2</sub>-C<sub>3</sub>H<sub>6</sub>-SCR over Ag/Al<sub>2</sub>O<sub>3</sub> catalysts.

Fig. 5 presents Arrhenius plots of the reaction rate for NOx conversion over Ag/Al<sub>2</sub>O<sub>3</sub> samples with varying silver loadings. Based on these results, the apparent activation energies (E<sub>a</sub>) for NOx conversion under the employed experimental conditions were calculated, with results listed in Table 2. Over all the Ag/Al<sub>2</sub>O<sub>3</sub> samples, the E<sub>a</sub> values for the H<sub>2</sub>-C<sub>3</sub>H<sub>6</sub>-SCR varied from 49.9 to 66.1 kJ/mol (Fig. 5A and Table 2), consistent with the literature [13,31]. For a given sample, introduction of water vapor induced a slight decrease in the value of E<sub>a</sub> (Fig. 5B and Table 2). The E<sub>a</sub> for NOx reduction in the absence of H<sub>2</sub> was also measured over 2 wt% and 4 wt% Ag/Al<sub>2</sub>O<sub>3</sub> (Fig. 5C). In this case, the presence of water vapor resulted in an increase of ca. 40 kJ/mol in the E<sub>a</sub> value for NOx reduction. Therefore, it can be speculated that water vapor did not change the pathway of the H<sub>2</sub>-assisted C<sub>3</sub>H<sub>6</sub>-SCR over Ag/Al<sub>2</sub>O<sub>3</sub> catalysts. To further reveal the role of water vapor in H<sub>2</sub>-C<sub>3</sub>H<sub>6</sub>-SCR, the following studies focused on the 2 wt% and 4 wt% Ag/Al<sub>2</sub>O<sub>3</sub> catalysts.

#### 3.3.2. Reaction order for NOx reduction

Fig. 6 and Table 3 show the dependence of the NOx conversion rate on the concentrations of NO and C<sub>3</sub>H<sub>6</sub> over Ag/Al<sub>2</sub>O<sub>3</sub> at 280 °C. Over 2 wt% Ag/Al<sub>2</sub>O<sub>3</sub>, the empirical reaction order of NO for NOx reduction in the presence of H<sub>2</sub> was 0.56. This result indicates a possibility that the reaction rate is substantially controlled by the surface reaction [1–3,5]. Over this catalyst, introduction of water

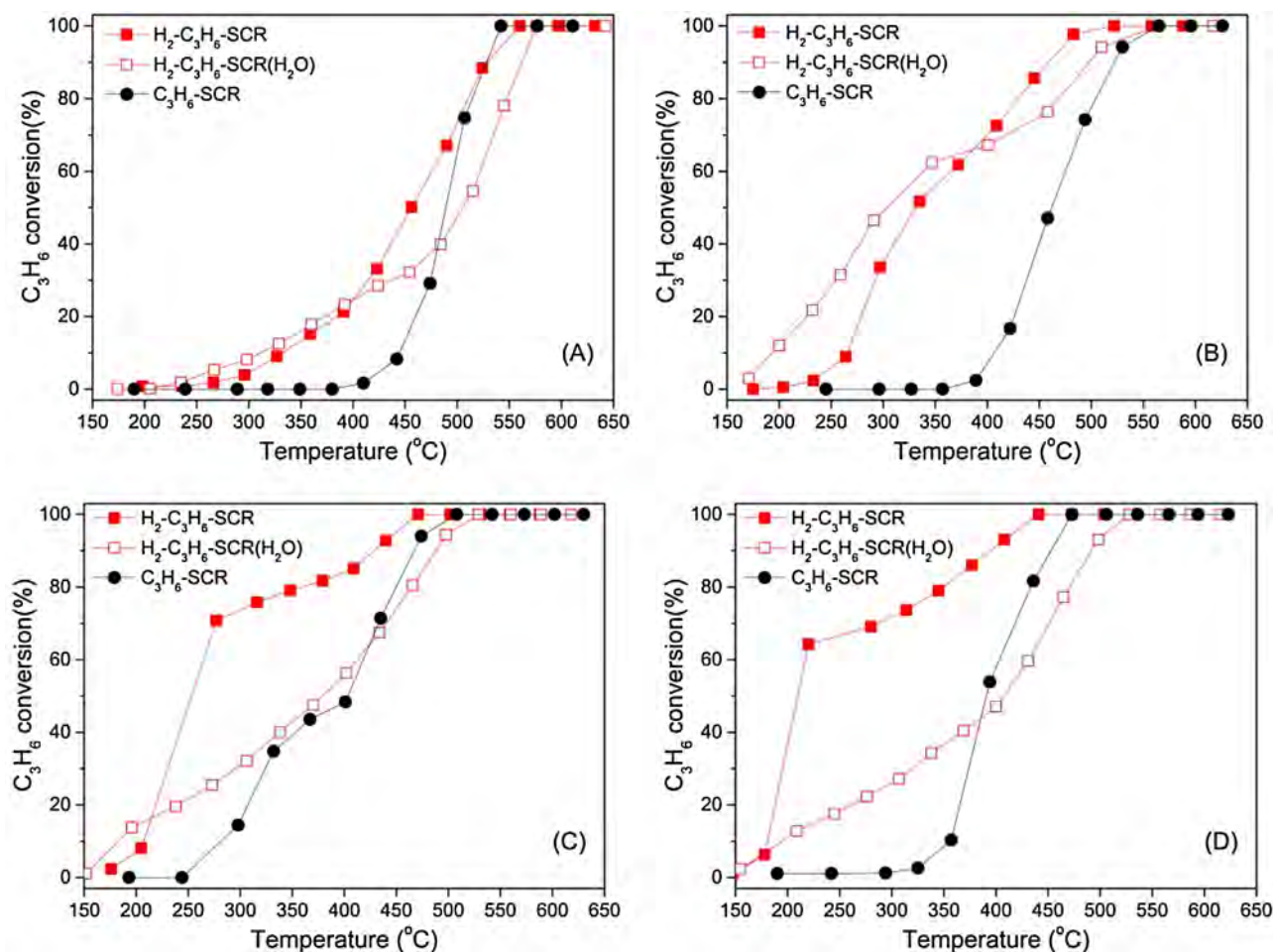


**Fig. 3.**  $C_3H_6$  conversions over (A) 1 wt%  $Ag/Al_2O_3$ , (B) 2 wt%  $Ag/Al_2O_3$ , (C) 4 wt%  $Ag/Al_2O_3$ , and (D) 6 wt%  $Ag/Al_2O_3$  under different conditions:  $H_2-C_3H_6-SCR$  (■),  $H_2-C_3H_6-SCR$  with water (□), and  $C_3H_6-SCR$  (●). The feed composition was the same as Fig. 2.

**Table 2**  
Apparent activation energy ( $E_a$ ) for  $NO_x$  conversion over  $Ag/Al_2O_3$ .

Sample	Activation energy (kJ/mol)		Reductant	Ref.
	0% $H_2O$	10% $H_2O$		
1 wt% $Ag/Al_2O_3$	49.9	46.1	$H_2+C_3H_6$	This work
2 wt% $Ag/Al_2O_3$	62.3	60.2	$H_2+C_3H_6$	This work
	74.1	115.4	$C_3H_6$	This work
4 wt% $Ag/Al_2O_3$	66.1	61.6	$H_2+C_3H_6$	This work
	80.3	122.8	$C_3H_6$	This work
6 wt% $Ag/Al_2O_3$	60.4	55.6	$H_2+C_3H_6$	This work
2 wt% $Ag/Al_2O_3$	61		$H_2+C_3H_8$	[13]
	224		$C_3H_8$	[13]
2.2 wt% $Ag/Al_2O_3$	26		$H_2+C_3H_6$	[31]
	105		$C_3H_6$	[31]

**Table 3**  
Reaction orders for  $NO_x$  conversion over  $Ag/Al_2O_3$ .

	$H_2-C_3H_6-SCR$		$H_2O-H_2-C_3H_6-SCR$	
	2 wt% $Ag/Al_2O_3$	4 wt% $Ag/Al_2O_3$	2 wt% $Ag/Al_2O_3$	4 wt% $Ag/Al_2O_3$
Order in $NO^a$	0.56	0.72	0.40	0.65
Order in $C_3H_6^b$	-0.62	0.56	0.73	0.73

<sup>a</sup>  $NO$  concentration range is 200 ppm to 1000 ppm.

<sup>b</sup>  $C_3H_6$  concentration range is 800 ppm to 2000 ppm.

vapor slightly decreased the reaction order of  $NO$  to 0.40. As for the 4 wt%  $Ag/Al_2O_3$ , the effect of water vapor on the  $NO$  reaction order was marginal, giving the value of 0.72 under water-free conditions

and 0.65 in the presence of moisture. As shown in Fig. 6B, surprisingly, the addition of water vapor increased the  $C_3H_6$  reaction order from a negative value (-0.62) to a positive value (0.73) over 2 wt%

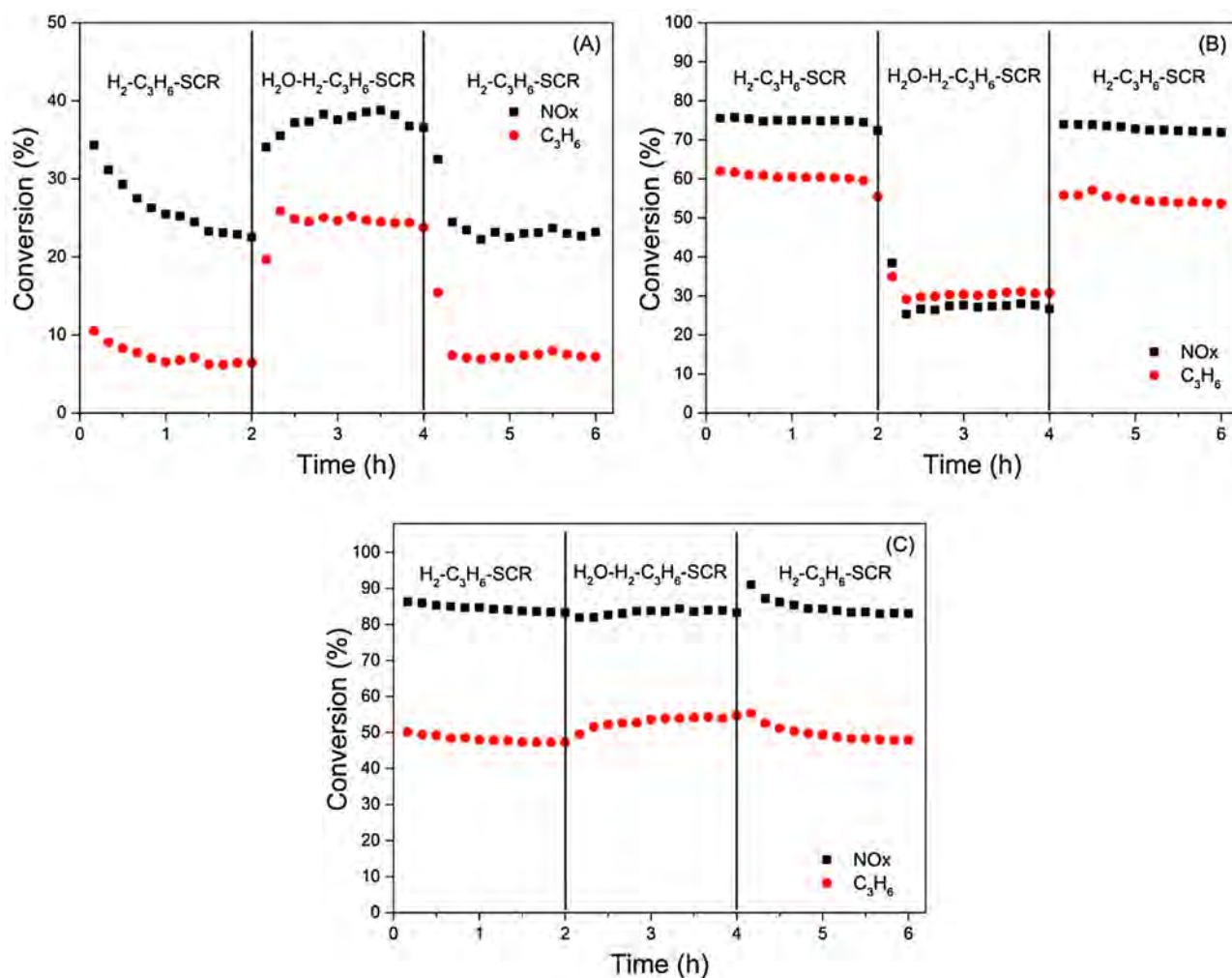


**Fig. 4.** Step-response experiment over (A) 2 wt% Ag/Al<sub>2</sub>O<sub>3</sub> at a GHSV = 100,000 (weight of catalyst = 0.3 g), (B) 4 wt% Ag/Al<sub>2</sub>O<sub>3</sub> at a GHSV = 300,000 (weight of catalyst = 0.1 g) at 265 °C, and (C) 2 wt% Ag/Al<sub>2</sub>O<sub>3</sub> at a GHSV = 300,000 (weight of catalyst = 0.1 g) at 400 °C in the fixed-bed reactor. Feed composition: NO 800 ppm, C<sub>3</sub>H<sub>6</sub> 1714 ppm, H<sub>2</sub> 1%, O<sub>2</sub> 10%, H<sub>2</sub>O 10% (when added), N<sub>2</sub> balance.

Ag/Al<sub>2</sub>O<sub>3</sub>. This result indicates that under water-free conditions, the reaction rate for NO<sub>x</sub> conversion decreased with increasing C<sub>3</sub>H<sub>6</sub> concentration, while this apparent poisoning effect was overcome by the introduction of water vapor, further confirming the enhancement effect of water vapor on NO<sub>x</sub> conversion (Fig. 2B) and C<sub>3</sub>H<sub>6</sub> conversion (Fig. 3B). Over 4 wt% Ag/Al<sub>2</sub>O<sub>3</sub>, however, the reaction order of C<sub>3</sub>H<sub>6</sub> was slightly increased by the addition of water vapor (from 0.56 to 0.73), indicating that the surface reaction involved in C<sub>3</sub>H<sub>6</sub> oxidation was retarded by water vapor, which was also in agreement with the results of activity testing (Fig. 3C).

The results of kinetic studies show that the introduction of water vapor does not change the apparent activation energy of NO<sub>x</sub> reduction in H<sub>2</sub>-assisted C<sub>3</sub>H<sub>6</sub>-SCR, indicating that the reaction pathway for NO<sub>x</sub> reduction remains the same over 2 wt% and 4 wt% Ag/Al<sub>2</sub>O<sub>3</sub>. Over the two catalysts, however, the effect of water vapor on the C<sub>3</sub>H<sub>6</sub> reaction order was distinctly different. This result possibly suggests that the adsorption and activation of C<sub>3</sub>H<sub>6</sub> are closely related to water vapor. To highlight this issue, further *in situ* DRIFTS measurements were performed, as presented in the next section.

### 3.4. *In situ* DRIFTS studies for NO<sub>x</sub> reduction by C<sub>3</sub>H<sub>6</sub>

#### 3.4.1. Influence of H<sub>2</sub>O on the partial oxidation of C<sub>3</sub>H<sub>6</sub>

Generally, the process of HC-SCR over Ag/Al<sub>2</sub>O<sub>3</sub> begins with the partial oxidation of hydrocarbons to produce reactive species

[1,15,21,56]. Therefore, the *in situ* DRIFTS of 2 wt% Ag/Al<sub>2</sub>O<sub>3</sub> during exposure to H<sub>2</sub>+C<sub>3</sub>H<sub>6</sub>+O<sub>2</sub> was measured first, with the results shown in Fig. 7. In this case, characteristic peaks due to surface species originating from the partial oxidation of C<sub>3</sub>H<sub>6</sub> were observed at the temperature of 150 °C (Fig. 7A). The peaks at 1591, 1394, and 1375 cm<sup>-1</sup> are assigned to adsorbed formate [20]. The appearance of peaks at 1576 and 1458 cm<sup>-1</sup> indicates the formation of adsorbed acetates [18,22,29,57]. According to previous research works [35,41,58,59], the shoulder peak appearing at 1633 cm<sup>-1</sup> can be attributed to adsorbed enolic species. Keeping the structural features of surface enolates (C=C-O<sup>-</sup>) in mind, there should be two other characteristic vibration frequencies, located at around 1416 and 1336 cm<sup>-1</sup>. However, the low concentration of enolic species derived from the partial oxidation of C<sub>3</sub>H<sub>6</sub> might explain the absence of the two peaks. In addition, a shoulder peak at 1669 cm<sup>-1</sup> assignable to adsorbed acetone was observed over Ag/Al<sub>2</sub>O<sub>3</sub> [20,60].

If the reaction time is taken into account, one can easily find that formate was preferentially formed or was stable on the surface of catalysts: 1) it appeared first in the initial stage of partial oxidation of C<sub>3</sub>H<sub>6</sub>; and 2) the high-frequency peak (1591 cm<sup>-1</sup>) assignable to formate species always exhibited the strongest intensity. It was only after 50 min of exposure to H<sub>2</sub>+C<sub>3</sub>H<sub>6</sub>+O<sub>2</sub> that the characteristic peak (1633 cm<sup>-1</sup>) of enolic species appeared, indicative of its instability.

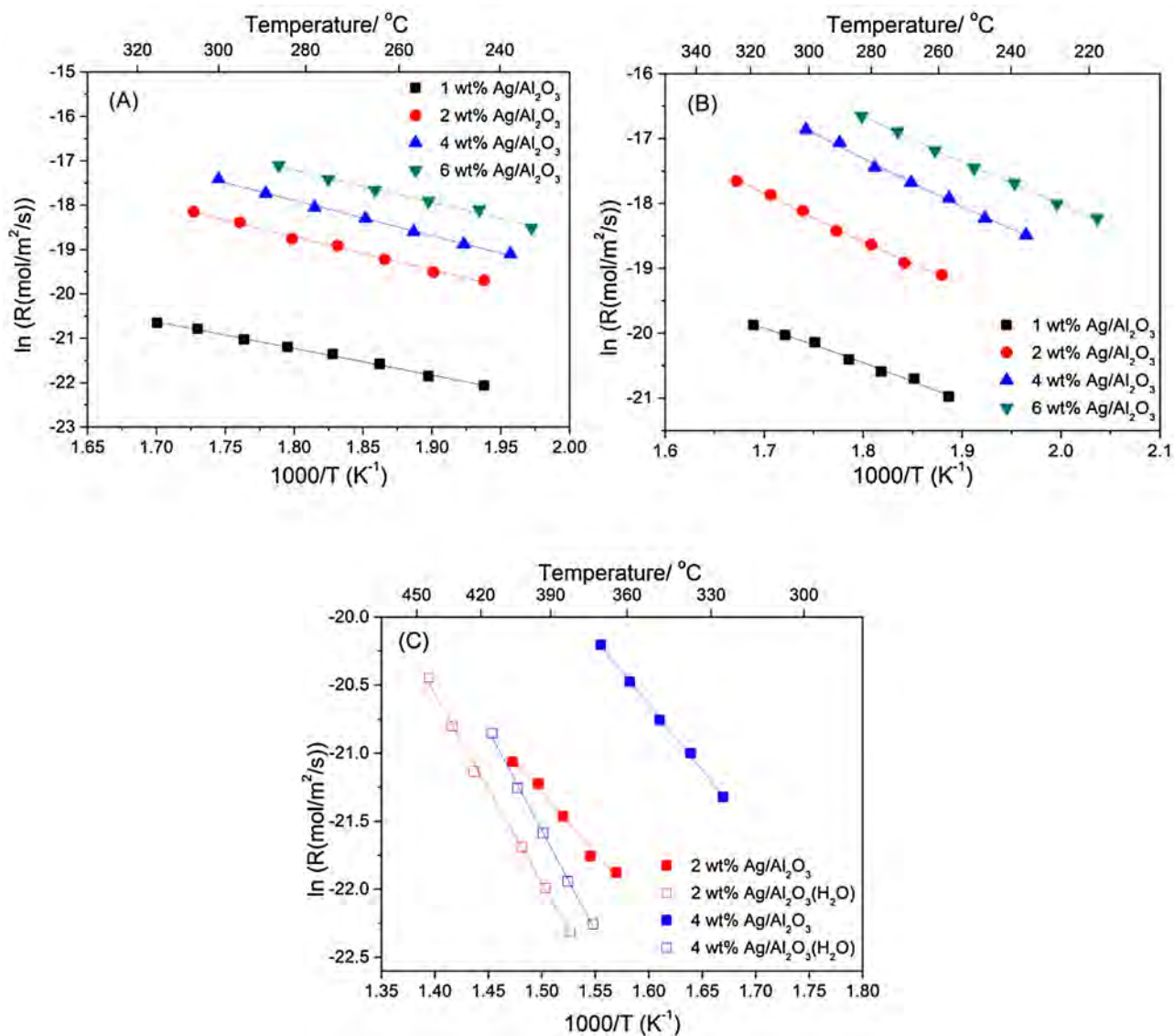


**Fig. 5.** Arrhenius plots for the rate of NO<sub>x</sub> conversion over Ag/Al<sub>2</sub>O<sub>3</sub> catalysts in different conditions (A) H<sub>2</sub>-C<sub>3</sub>H<sub>6</sub>-SCR without water vapor, (B) H<sub>2</sub>-C<sub>3</sub>H<sub>6</sub>-SCR with water vapor, and (C) C<sub>3</sub>H<sub>6</sub>-SCR with or without water vapor. Feed composition: 800 ppm NO, 1714 ppm C<sub>3</sub>H<sub>6</sub>, 10% O<sub>2</sub>, 1% H<sub>2</sub> (when added), 10% H<sub>2</sub>O (when added), and N<sub>2</sub> balance. GHSV: varying in the range of 100,000–3,000,000 h<sup>-1</sup> in order to obtain NO<sub>x</sub> conversion below 20%.

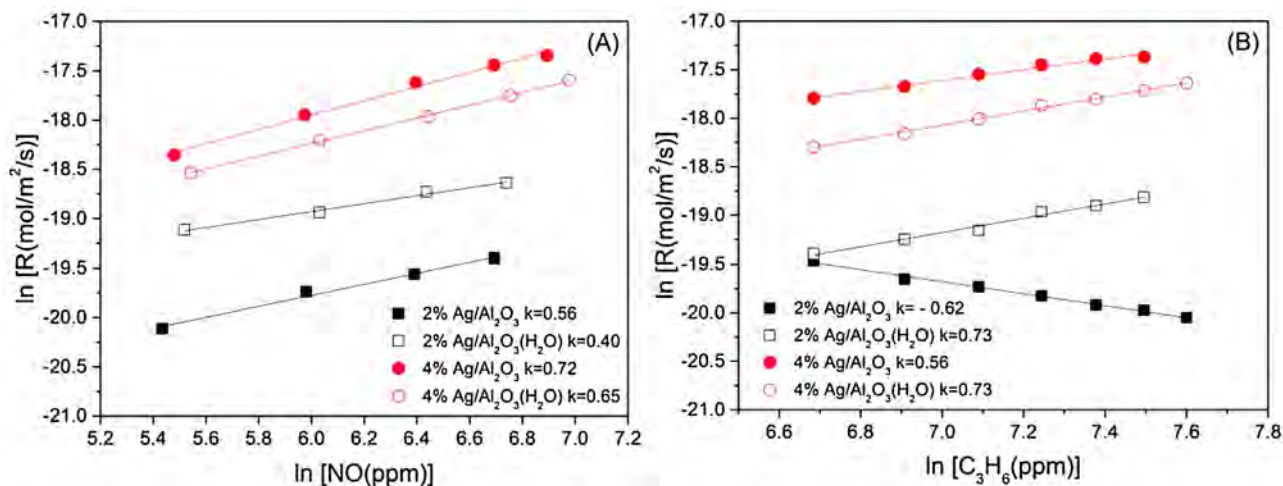


**Fig. 6.** Reaction rates of NO<sub>x</sub> conversion as a function of (A) NO and (B) C<sub>3</sub>H<sub>6</sub> concentration over Ag/Al<sub>2</sub>O<sub>3</sub> at 280 °C.

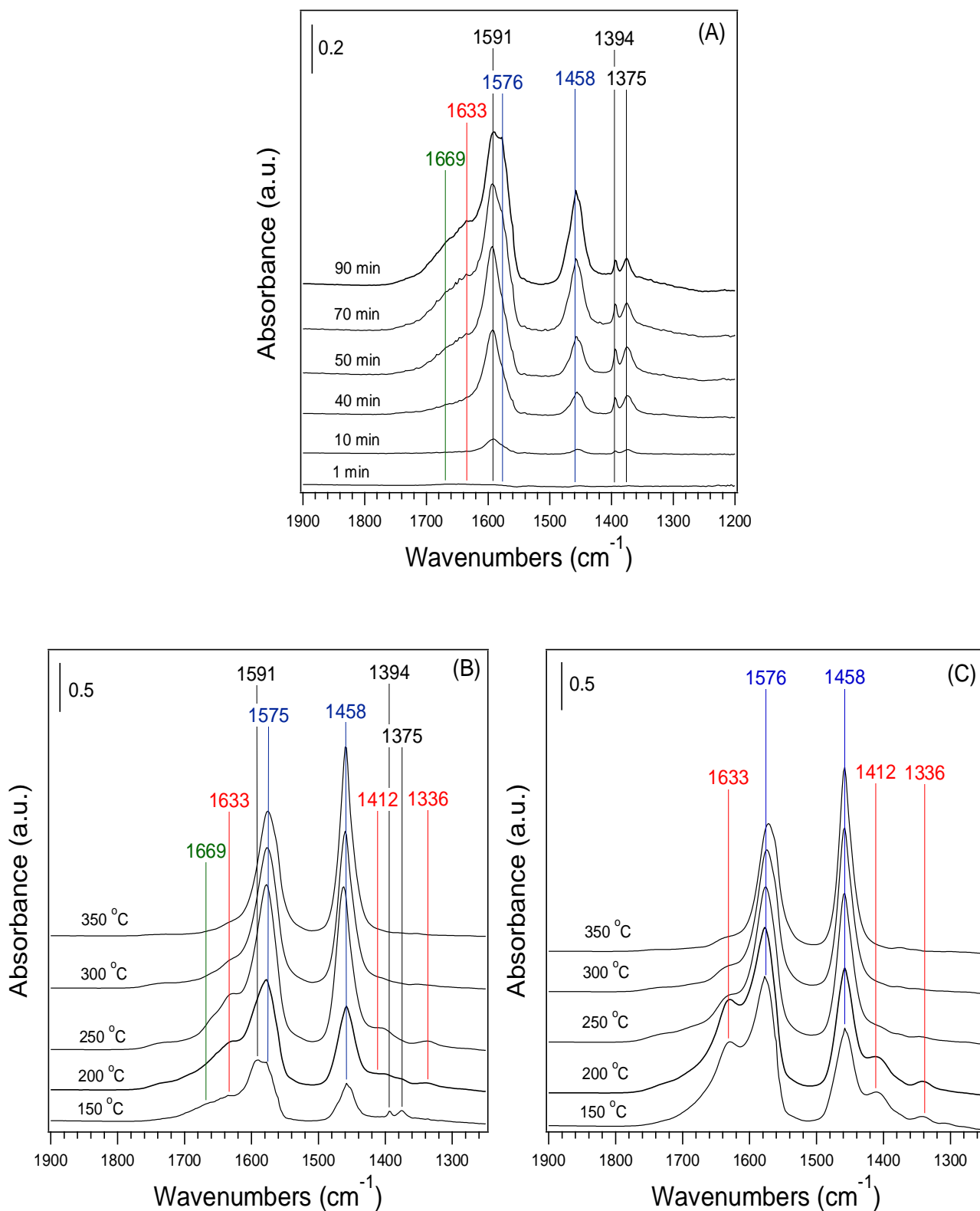


**Fig. 7.** Dynamic change of *in situ* DRIFTS spectra of adsorbed species on 2 wt% Ag/Al<sub>2</sub>O<sub>3</sub> during the oxidation of C<sub>3</sub>H<sub>6</sub> in the presence of H<sub>2</sub> at 150 °C (A). *In situ* DRIFTS spectra of adsorbed species on (B) 2 wt% Ag/Al<sub>2</sub>O<sub>3</sub> and (C) 4 wt% Ag/Al<sub>2</sub>O<sub>3</sub> in steady states in a flow of C<sub>3</sub>H<sub>6</sub> + H<sub>2</sub> + O<sub>2</sub> at different temperatures. Feed composition: C<sub>3</sub>H<sub>6</sub> 1714 ppm, H<sub>2</sub> 1%, O<sub>2</sub> 10%, N<sub>2</sub> balance.

Under the same gas feed conditions, the *in situ* DRIFTS spectra of 2 wt% Ag/Al<sub>2</sub>O<sub>3</sub> was further measured at elevated temperatures (Fig. 7B). As temperature increased, the intensities of peaks due to formate significantly decreased, and disappeared at tempera-

tures above 250 °C. In contrast, the intensity of peaks due to acetate species distinctly increased, becoming predominant at temperatures above 250 °C. The peak at 1633 cm<sup>-1</sup> increased in intensity as temperature increased from 150 °C to 250 °C, indicating an increase

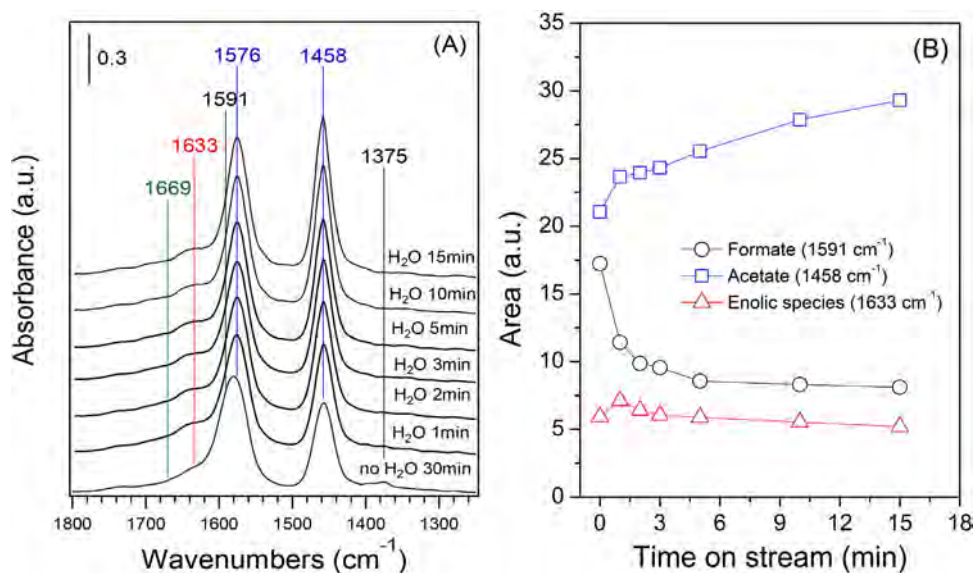


**Fig. 8.** Dynamic changes of *in situ* DRIFTS spectra of adsorbed species over 2 wt% Ag/Al<sub>2</sub>O<sub>3</sub> as a function of time in a flow of H<sub>2</sub>O + H<sub>2</sub> + C<sub>3</sub>H<sub>6</sub> + O<sub>2</sub> at 265 °C (A), and (B) the integrated areas of the peaks due to formate (1591 cm<sup>-1</sup>), acetate (1458 cm<sup>-1</sup>), and enolic species (1633 cm<sup>-1</sup>) in the case of (A). Before measurement, the catalyst was pre-exposed to a flow of H<sub>2</sub> + C<sub>3</sub>H<sub>6</sub> + O<sub>2</sub> for 30 min at 265 °C. Feed composition: C<sub>3</sub>H<sub>6</sub> 1714 ppm, H<sub>2</sub> 1%, O<sub>2</sub> 10%, H<sub>2</sub>O 5% (when added), N<sub>2</sub> balance.

in the concentration of surface enolic species. This increase was accompanied by the appearance of low-frequency bands at 1412 and 1336 cm<sup>-1</sup> due to the enolic species. Raising the reaction temperature further lowered the concentration of enolic species over 2 wt% Ag/Al<sub>2</sub>O<sub>3</sub>.

The same set of DRIFTS measurements was also carried out over 4 wt% Ag/Al<sub>2</sub>O<sub>3</sub>, with the results shown in Fig. 7C. Notably, the characteristic peaks assignable to formate were hardly observed, while those of acetate (1576 and 1458 cm<sup>-1</sup>) were predominant over the whole temperature range. Characteristic frequencies of enolic species were clearly observed at 1633, 1412, and 1336 cm<sup>-1</sup> at temperatures between 150 °C and 200 °C. Within this temperature range, meanwhile, the highest-frequency peak of the enolic species exhibited much stronger intensity compared with the results presented in Fig. 7B.

The effect of moisture content on the partial oxidation of C<sub>3</sub>H<sub>6</sub> over 2 wt% Ag/Al<sub>2</sub>O<sub>3</sub> was further studied by *in situ* DRIFTS at 265 °C (Fig. 8A). In order to clarify the dynamic change of surface intermediates induced by the introduction of water vapor, the spectra (Fig. 8A) in the range of 1200–1800 cm<sup>-1</sup> were then fitted and deconvoluted to the constituent peaks (with typical results presented in Fig. S7). The integrated areas of peaks at 1591 cm<sup>-1</sup> (for formate), 1458 cm<sup>-1</sup> (for acetate), and 1633 cm<sup>-1</sup> (for enolic species) are plotted as a function of time-on-stream (Fig. 8B). As can be seen from Fig. 8A, after exposure of 2 wt% Ag/Al<sub>2</sub>O<sub>3</sub> to a gas mixture of H<sub>2</sub> + C<sub>3</sub>H<sub>6</sub> + O<sub>2</sub> for 30 min, strong peaks due to formate (1591 cm<sup>-1</sup>) and acetate (1458 and 1576 cm<sup>-1</sup>) were observed, along with the generation of enolic species (1633 cm<sup>-1</sup>). The addition of water vapor significantly decreased the intensity of the peaks due to formate in the first 2 min, followed by more gradual decrease (Fig. 8B). As the concentration of formate decreased, the intensity of enolic species was slightly increased in the initial 1 min of water introduction, and then decreased slowly. During the entire process of water addition, meanwhile, a monotonic increase in the intensity of acetate was observed over 2 wt% Ag/Al<sub>2</sub>O<sub>3</sub>.

#### 3.4.2. Influence of H<sub>2</sub>O on H<sub>2</sub>-C<sub>3</sub>H<sub>6</sub>-SCR over Ag/Al<sub>2</sub>O<sub>3</sub>

Over the 2 wt% Ag/Al<sub>2</sub>O<sub>3</sub>, the kinetic study (Fig. 6 and Table 3) showed that the reaction order of C<sub>3</sub>H<sub>6</sub> for H<sub>2</sub>-C<sub>3</sub>H<sub>6</sub>-SCR was -0.62, indicating that certain products derived from C<sub>3</sub>H<sub>6</sub> par-

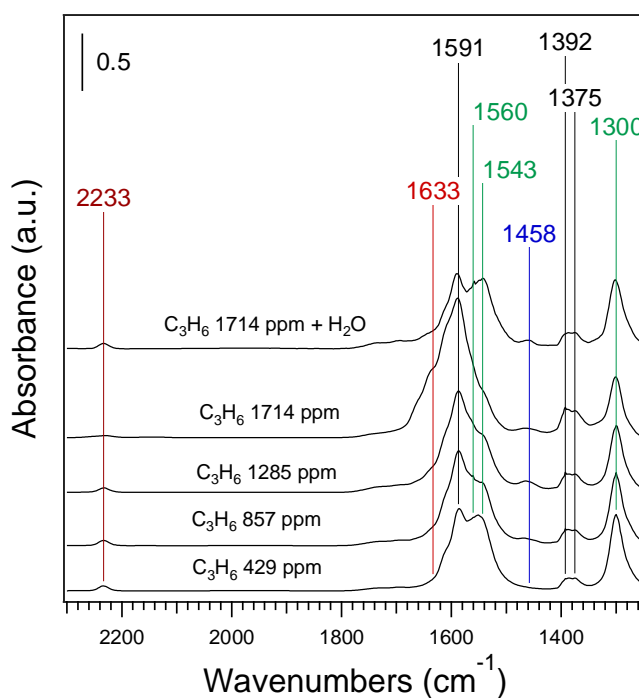


**Fig. 9.** DRIFTS spectra of adsorbed species during H<sub>2</sub>-C<sub>3</sub>H<sub>6</sub>-SCR with varying C<sub>3</sub>H<sub>6</sub> concentration over 2 wt% Ag/Al<sub>2</sub>O<sub>3</sub> at steady state at 265 °C. Feed composition: NO 800 ppm, C<sub>3</sub>H<sub>6</sub> from 429 to 1714 ppm, H<sub>2</sub> 1%, O<sub>2</sub> 10%, H<sub>2</sub>O 5% (when added), N<sub>2</sub> balance.

tial oxidation inhibited the reduction of NO<sub>x</sub>. To highlight this issue, an *in situ* DRIFTS experiment was carried out under H<sub>2</sub>-C<sub>3</sub>H<sub>6</sub>-SCR conditions while increasing the concentration of C<sub>3</sub>H<sub>6</sub> from 429 ppm to 1714 ppm (Fig. 9). As the C<sub>3</sub>H<sub>6</sub> concentration increased, notably, the intensities of the peaks due to formate (1591, 1392, and 1375 cm<sup>-1</sup>) distinctly increased, indicating that the formate coverage strongly depended on the C<sub>3</sub>H<sub>6</sub> concentration. During this process, increased intensities of peaks assignable to acetate (1458 cm<sup>-1</sup>) and enolic species (1633 cm<sup>-1</sup>) were also observed, while their intensities, particularly for the acetate, were

much lower than that of formate. Also,  $-\text{NCO}$  ( $2233\text{ cm}^{-1}$ ), monodentate nitrate ( $1560\text{--}1543\text{ cm}^{-1}$ ), and isolated bidentate nitrate ( $1300\text{ cm}^{-1}$ ) were observed [2,15,61]. It has been widely accepted that the  $-\text{NCO}$  species, derived from the reaction between adsorbed nitrates and oxygenated HC species (including enolic species and acetate), is a key intermediate in the HC-SCR of NOx over  $\text{Ag}/\text{Al}_2\text{O}_3$  [1,2,62]. The  $-\text{NCO}$  species shows high reactivity toward  $\text{NO} + \text{O}_2$  to produce  $\text{N}_2$ , the appearance of which thus indicates that the global NOx reduction process has occurred. An increased intensity of  $-\text{NCO}$  species was observed after water vapor was introduced into the gas mixture, indicative of the enhancement for NOx reduction, which was in agreement with the activity result (Fig. 4).

Over  $\text{Ag}/\text{Al}_2\text{O}_3$ , our previous study [20] showed that  $\text{C}_3\text{H}_6$  was more efficient for NOx reduction than  $\text{CH}_4$ . Formate, as the main product of partial oxidation of  $\text{CH}_4$ , exhibited low reactivity toward  $\text{NO} + \text{O}_2$  to produce  $-\text{NCO}$ , finally leading to a low deNOx activity for  $\text{CH}_4$  over  $\text{Ag}/\text{Al}_2\text{O}_3$ . The acetate and enolic species exhibit higher activity, thus playing an important role in  $\text{C}_3\text{H}_6$ -SCR and  $\text{H}_2$ - $\text{C}_3\text{H}_6$ -SCR, respectively [20]. With this in mind, it is clear that formate acts as a spectator in  $\text{H}_2$ - $\text{C}_3\text{H}_6$ -SCR, accumulating severely on the reaction sites of 2 wt%  $\text{Ag}/\text{Al}_2\text{O}_3$  and inhibiting the adsorption and subsequent activation of other reactants, thus contributing to a negative reaction order of  $\text{C}_3\text{H}_6$  for NOx reduction. Addition of water vapor significantly decreased the formate coverage on the surface of the silver catalyst, giving more sites available for other active intermediates, and thus increased SCR activity. Similarly, a negative reaction order of NO ( $-2.53$ ) for  $\text{C}_3\text{H}_8$ -SCR was observed by Shimizu et al. [13], the occurrence of which was induced by nitrate coverage on the surface of  $\text{Ag}/\text{Al}_2\text{O}_3$ . Further research indicated that addition of hydrogen was effective in decreasing nitrate coverage, leading to a positive value of NO reaction order (0.49).

As shown in Fig. 8A, formate, acetate and enolic species adsorbed on the surface of 2 wt%  $\text{Ag}/\text{Al}_2\text{O}_3$  were produced by the partial oxidation of  $\text{C}_3\text{H}_6$ . The produced enolic species and acetate exhibit high activity towards  $\text{NO} + \text{O}_2$ , leaving the inert formate on the surface of the silver catalyst. As a result, formate was predominant during the  $\text{H}_2$ - $\text{C}_3\text{H}_6$ -SCR process (Fig. 9). Introduction of water vapor into  $\text{H}_2 + \text{C}_3\text{H}_6 + \text{O}_2$  enhanced the generation of enolic species and acetate (Fig. 8A and B). The enolic species was clearly observed during  $\text{H}_2$ - $\text{C}_3\text{H}_6$ -SCR over 2 wt%  $\text{Ag}/\text{Al}_2\text{O}_3$ , while the acetate exhibited a low concentration (Fig. 9). Introduction of water vapor into the gas feed of  $\text{H}_2$ - $\text{C}_3\text{H}_6$ -SCR significantly decreased the intensity of enolic species, whereas it hardly changed the surface concentration of acetate. During the  $\text{H}_2$ - $\text{C}_3\text{H}_6$ -SCR over 2 wt%  $\text{Ag}/\text{Al}_2\text{O}_3$ , activity measurement showed that water vapor introduction promoted NOx and  $\text{C}_3\text{H}_6$  conversion (Fig. 4A). As a result, it can be concluded that the decrease of enolic species concentration induced by the introduction of water vapor into the  $\text{H}_2$ - $\text{C}_3\text{H}_6$ -SCR system was derived from accelerated consumption of enolic species. This result, in turn, suggests that the pathway involving the generation of enolic species and its further transformation plays a crucial role in the  $\text{H}_2$ - $\text{C}_3\text{H}_6$ -SCR process over 2 wt%  $\text{Ag}/\text{Al}_2\text{O}_3$ , particularly at low temperatures.

### 3.5. DFT calculations

Kinetic studies and *in situ* DRIFTS measurements confirmed that water vapor significantly changed the behaviors of surface formate, acetate, and enolic species, thus contributing to the activity of 2 wt%  $\text{Ag}/\text{Al}_2\text{O}_3$  for  $\text{H}_2$ - $\text{C}_3\text{H}_6$ -SCR. To highlight this issue, the adsorption of these species on a  $\text{Ag}/\text{Al}_2\text{O}_3$  slab and hydroxylated  $\text{Ag}/\text{Al}_2\text{O}_3$  slab was calculated. Over this catalyst, UV-vis spectra clearly showed that the silver cations were predominant. According to our previous NMR and DFT calculations, silver ions over 2 wt%  $\text{Ag}/\text{Al}_2\text{O}_3$  might be bound on tetra- and octa-coordinate Al sites, forming  $\text{Ag-O-Al}_{\text{octa}}$

(on  $\text{Ag}/\text{Al}_2\text{O}_3$  (100) surface) and  $\text{Ag-O-Al}_{\text{tetra}}$  (on  $\text{Ag}/\text{Al}_2\text{O}_3$  (110) surface) entities. As a result, periodic models of  $\text{Ag}/\text{Al}_2\text{O}_3$  catalysts and their hydroxylated counterparts containing these two structural features were established (Fig. S2). Over  $\text{Ag}/\text{Al}_2\text{O}_3$ , *in situ* DRIFTS and the corresponding calculation results confirmed that the enolic species was preferentially linked with Ag sites, while the acetate tended to adsorb on Al sites [35]. Over pure  $\text{Al}_2\text{O}_3$ , the partial oxidation of  $\text{C}_3\text{H}_6$  in the presence of  $\text{H}_2$  was also measured by *in situ* DRIFTS, with the results shown in Fig. S8. In this case, it should be noted that the formate exhibits the same characteristic frequencies peaks as those on  $\text{Ag}/\text{Al}_2\text{O}_3$ , strongly suggesting that the formate is preferentially linked with Al sites. Keeping such intrinsic properties in mind, periodic models for the adsorbed enolic species, acetate, and formate on the  $\text{Ag}/\text{Al}_2\text{O}_3$  surface were established and the relaxed structures are shown in Figs. S9–S11, respectively.

The DFT-calculated adsorption energies are summarized in Table 4. All of the adsorption energies had negative values, which indicates that the surface has a strong affinity for the formate, acetate, and enolic species. For the dehydrated  $\text{Ag}/\text{Al}_2\text{O}_3$  surface, the adsorption energies of formate, acetate, and enolic species on the  $\text{Ag}/\text{Al}_2\text{O}_3$  (110) surface are more negative than on the  $\text{Ag}/\text{Al}_2\text{O}_3$  (100) surface, which indicates that these species are preferentially adsorbed on the (110) surface. Previous theoretical calculations and experimental results showed that the (110) surface predominates on  $\gamma\text{-Al}_2\text{O}_3$ , with about 70% of the total area, followed by the (100) surface ( $\sim 20\%$ ) [63,64]. The adsorption energies of formate ( $-2.84\text{ eV}$ ) and acetate ( $-3.09\text{ eV}$ ) were significantly more negative than that of the enolic species ( $-1.99\text{ eV}$ ), meaning that formate and acetate are more easily formed on the (110) surface, which is consistent with the results of DRIFTS.

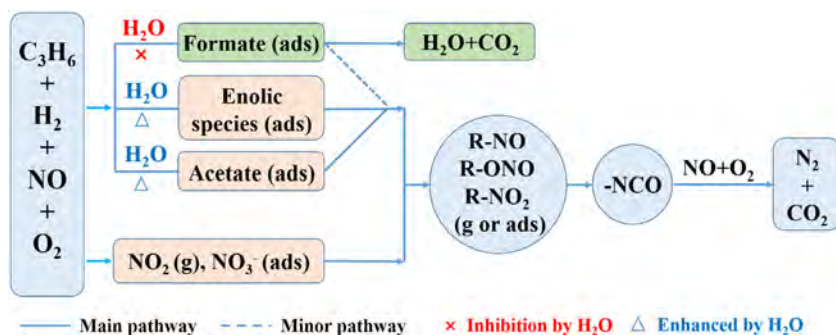
On the hydroxylated  $\text{Ag}/\text{Al}_2\text{O}_3$  (110) surface, the values of adsorption energies for all of the three species became less negative compared to those on the dehydrated  $\text{Ag}/\text{Al}_2\text{O}_3$  surface, meaning the adsorption of these species will be weakened. Such weakening was consistent with a final decreased intensity of IR adsorption bands assignable to the formate and enolic species derived from water vapor addition (Fig. 8). For the acetate species adsorbed on the hydroxylated  $\text{Ag}/\text{Al}_2\text{O}_3$  (110) surface, the 55% weakening of the adsorption energy seems contradictory with the increase of the integrated areas of the IR peak induced by water introduction. On the  $\text{Ag}/\text{Al}_2\text{O}_3$  (100) surface, however, the presence of hydroxyl groups leads to an obvious strengthening (42%) of the adsorption energy of acetate. These results suggest that the adsorption of acetate on the (100) surface is much more favorable than that on the (110) surface in the presence of hydroxyl groups. As a result, it is reasonable that the amount of acetate was increased in the presence of moisture. As can be seen from Table 4, also, the adsorption energy for formate on the (100) surface is more negative in the presence of hydroxyl, whereas the adsorption of formate ( $-3.70\text{ eV}$ ) is still weaker than that of acetate ( $-3.84\text{ eV}$ ). This means that the adsorption of formate is more difficult on the (100) surface considering its competitive adsorption with acetate for the same Al sites.

During the partial oxidation of  $\text{C}_3\text{H}_6$  over 2 wt%  $\text{Ag}/\text{Al}_2\text{O}_3$  (Fig. 8), it should be noted that an increased intensity of enolic species was clearly observed in the initial stage of water introduction, followed by a slow decrease. After 5 min of water addition, the concentration of enolic species was lower than that under water-free condition. Such dynamic behavior of enolic species triggered by water vapor addition can be explained as follows. As shown in Fig. S8 and S10, although the enolic species and formate were adsorbed on different sites (the enolic species was bound on Ag sites while the formate adsorbed on Al sites), a high concentration of formate would result in a strong steric effect on the adsorption of enolic species. This steric effect would occur during the partial oxidation of  $\text{C}_3\text{H}_6$  without water vapor. Introduction of water vapor

**Table 4**  
DFT-calculated adsorption energies.

Model	adsorption energy (eV)		
	HCOO <sup>-</sup>	CH <sub>2</sub> =CHO <sup>-</sup>	CH <sub>3</sub> COO <sup>-</sup>
Ag/Al <sub>2</sub> O <sub>3</sub> (110)	-2.84	-1.99	-3.09
20OH-Ag/Al <sub>2</sub> O <sub>3</sub> (110)	-1.62 (-43%)	-1.40 (-30%)	-1.39 (-55%)
Ag/Al <sub>2</sub> O <sub>3</sub> (100)	-2.78	-1.95	-2.71
12OH-Ag/Al <sub>2</sub> O <sub>3</sub> (100)	-3.70 (33%)	-1.86 (-4%)	-3.84 (42%)

The number in brackets is the change percentage.



**Scheme 1.** Proposed interpretation of water influence on the H<sub>2</sub> assisted C<sub>3</sub>H<sub>6</sub>-SCR over Ag/Al<sub>2</sub>O<sub>3</sub>.

significantly decreased the concentration of formate over Ag/Al<sub>2</sub>O<sub>3</sub>, reducing the steric effect and enabling more silver sites to be available for enolic species. As a result, an increased intensity of enolic species appeared in the initial stage of water introduction. On the other hand, water vapor addition induced hydroxylation of the Ag/Al<sub>2</sub>O<sub>3</sub> surface, the occurrence of which decreases the adsorption energy of enolic species. Thus, it is reasonable that the concentration of surface enolic species in the final stage of water vapor addition was lower than that under water-free conditions.

#### 4. Discussion

Over the 4 wt% Ag/Al<sub>2</sub>O<sub>3</sub> catalyst, DRIFTS and GC-MS measurements revealed that the enolic species produced by the partial oxidation of C<sub>3</sub>H<sub>6</sub> in the presence of H<sub>2</sub> showed high activity for reaction with NO+O<sub>2</sub> to form N<sub>2</sub>, which can be considered to occur as follows: C<sub>3</sub>H<sub>6</sub> + H<sub>2</sub> + NO + O<sub>2</sub> → ad-NOx + enolic species (acetate also formed) → R-ONO + R-NO<sub>2</sub> → -NCO + -CN → N<sub>2</sub> [15,20]. During this process, acetate was also produced, which exhibited a lower activity than enolic species; thus the pathway involving the generation of enolic species and their further reaction governs the H<sub>2</sub>-C<sub>3</sub>H<sub>6</sub>-SCR process, particularly in the low temperature region. Over 2 wt% Ag/Al<sub>2</sub>O<sub>3</sub>, the kinetic studies presented here show that the apparent activation energy for NOx reduction was almost the same as that obtained with 4 wt% Ag/Al<sub>2</sub>O<sub>3</sub>, indicative of a similar pathway of NOx reduction (Scheme 1). Over 2 wt% Ag/Al<sub>2</sub>O<sub>3</sub>, formate also formed during the partial oxidation of C<sub>3</sub>H<sub>6</sub>, while this species exhibited low activity toward NO+O<sub>2</sub>. During H<sub>2</sub>-C<sub>3</sub>H<sub>6</sub>-SCR, the produced enolic species and acetate were consumed by reaction with NO+O<sub>2</sub> (and/or surface nitrates), while the formate tended to accumulate seriously, thus exhibiting a poisoning effect on the reduction of NOx over 2 wt% Ag/Al<sub>2</sub>O<sub>3</sub>. The introduction of water vapor into the H<sub>2</sub>-C<sub>3</sub>H<sub>6</sub>-SCR system decreased the formate coverage, leaving more sites for the generation of active species (including enolic species and acetates) and also for their further reaction. As a result, the NOx reduction was promoted by water vapor addition over 2 wt% Ag/Al<sub>2</sub>O<sub>3</sub>, which was confirmed by the kinetic studies and *in situ* DRIFTS measurements.

UV-vis analysis revealed that silver cations (Ag<sup>+</sup>), oxidized silver clusters (Ag<sub>n</sub><sup>δ+</sup>), and metallic silver clusters (Ag<sub>n</sub><sup>0</sup>) were present

on the surface of Ag/Al<sub>2</sub>O<sub>3</sub>. As for the process of HC-SCR taking place over Ag/Al<sub>2</sub>O<sub>3</sub>, the oxidized silver species (Ag<sup>+</sup> and Ag<sub>n</sub><sup>δ+</sup>) contributed to partial oxidation of the reductant, thus serving as the active sites for NOx reduction. The metallic silver entities were often present on Ag/Al<sub>2</sub>O<sub>3</sub> with high silver content, promoting the complete oxidation of reductant to produce CO<sub>2</sub> [1,2,33,37]. As for 2 wt% Ag/Al<sub>2</sub>O<sub>3</sub>, oxidized silver species were predominant while the metallic entities exhibited a low proportion, thus the transformation of formate to CO<sub>2</sub> was difficult at low temperatures during the H<sub>2</sub>-C<sub>3</sub>H<sub>6</sub>-SCR. An increase in metallic silver clusters was clearly observed over 4 wt% Ag/Al<sub>2</sub>O<sub>3</sub>. This means that the 4 wt% Ag/Al<sub>2</sub>O<sub>3</sub> had stronger oxidizing ability than the catalyst with 2 wt% Ag loading, accelerating the decomposition of formate so that this inert species was hardly observed over the whole temperature region in the process of NOx reduction.

Water adsorption is inevitable on oxide surfaces, serving as a promoter/reactant or as an inhibitor in a given reaction taking place over oxide surfaces. Just by tuning the loading of silver, interestingly, quite opposite effects of water vapor were clearly observed over Ag/Al<sub>2</sub>O<sub>3</sub> catalysts for H<sub>2</sub>-C<sub>3</sub>H<sub>6</sub>-SCR. As for the water-gas shift reaction, molecular water would react with the key intermediate of surface formate to produce CO<sub>2</sub> and H<sub>2</sub> [65], which is quite different from our result. The theoretical calculation presented here shows that the presence of water can weaken the interactions between the Ag/Al<sub>2</sub>O<sub>3</sub> surface and the spectator species formate, thus more surface sites become available for the formation of active intermediates such as acetate.

Over Ag/Al<sub>2</sub>O<sub>3</sub> catalysts, it has been suggested that the addition of H<sub>2</sub> enhanced activation of O<sub>2</sub> to active oxygen species (e.g. O<sub>2</sub><sup>-</sup> and OOH species), and then benefited the partial oxidation of hydrocarbons and NOx reduction [21,66]. In our case, it is possible that the active oxygen species mentioned above would be produced during the H<sub>2</sub>-C<sub>3</sub>H<sub>6</sub>-SCR. On an oxide surface such as the Al<sub>2</sub>O<sub>3</sub> surface, meanwhile, dissociative adsorption of H<sub>2</sub>O molecules often occurs, providing an efficient pathway for the regeneration of active oxygen species [40]. With this in mind, the presence of water vapor also gives the possibility for the promotion of the H<sub>2</sub>-C<sub>3</sub>H<sub>6</sub>-SCR process, by regeneration of active oxygen species produced by O<sub>2</sub> activation.

## 5. Conclusion

Oxidized silver species contributed to the partial oxidation of  $C_3H_6$ , also serving as the active sites for  $H_2$ -assisted  $C_3H_6$ -SCR over  $Ag/Al_2O_3$ , while metallic silver clusters exhibited strong oxidizing properties and thus promoted the complete oxidation of the reductant to produce  $CO_2$ . Over 2 wt%  $Ag/Al_2O_3$ , oxidized silver species were predominant, with a small fraction of metallic silver. As a result, the 2 wt%  $Ag/Al_2O_3$  was highly active for  $H_2$ - $C_3H_6$ -SCR, whereas it was inactive for the low-temperature transformation of inert formate to  $CO_2$  in the absence of water vapor. In this case, a serious accumulation of formate thus induced a poisoning effect for  $NO_x$  conversion over 2 wt%  $Ag/Al_2O_3$ , the occurrence of which was confirmed by *in situ* DRIFTS and kinetic studies. *In situ* DRIFTS and DFT calculation studies further revealed that the water molecule may serve as a scavenger of inert formate; its addition therefore significantly decreased the formate coverage, giving more surface sites available for the generation of active enolic species and acetates, finally leading to an increase in the low-temperature activity of 2 wt%  $Ag/Al_2O_3$  for  $H_2$ - $C_3H_6$ -SCR.

## Acknowledgment

This work was supported by the National Natural Science Foundation of China (21373261, 21673277, and 21637005).

## Appendix A. Supplementary data

Supplementary data associated with this article can be found, in the online version, at <http://dx.doi.org/10.1016/j.apcatb.2017.02.001>.

## References

- [1] R. Burch, J.P. Breen, F.C. Meunier, Appl. Catal. B-Environ. 39 (2002) 283–303.
- [2] H. He, Y.B. Yu, Catal. Today 100 (2005) 37–47.
- [3] P. Granger, V.I. Parvulescu, Chem. Rev. 111 (2011) 3155–3207.
- [4] M.K. Kim, P.S. Kim, J.H. Baik, I.S. Nam, B.K. Cho, S.H. Oh, Appl. Catal. B-Environ. 105 (2011) 1–14.
- [5] K. Shimizu, A. Satsuma, Phys. Chem. Chem. Phys. 8 (2006) 2677–2695.
- [6] Z.M. Liu, S.I. Woo, Catal. Rev. 48 (2006) 43–89.
- [7] Z.M. Liu, J.H. Li, A.S.M. Junaid, Catal. Today 153 (2010) 95–102.
- [8] R. Burch, Catal. Rev. 46 (2004) 271–333.
- [9] J.H. Li, R. Ke, W. Li, J.M. Hao, Catal. Today 126 (2007) 272–278.
- [10] F. Gunnarsson, J.A. Pihl, T.J. Toops, M. Skoglundh, H. Harelind, Appl. Catal. B-Environ. 202 (2017) 42–50.
- [11] S. Satokawa, Chem. Lett. (2000) 294–295.
- [12] S. Satokawa, J. Shibata, K. Shimizu, S. Atsushi, T. Hattori, Appl. Catal. B-Environ. 42 (2003) 179–186.
- [13] K. Shimizu, J. Shibata, A. Satsuma, J. Catal. 239 (2006) 402–409.
- [14] S. Satokawa, J. Shibata, K.I. Shimizu, A. Satsuma, T. Hattori, T. Kojima, Chem. Eng. Sci. 62 (2007) 5335–5337.
- [15] X.L. Zhang, Y.B. Yu, H. He, Appl. Catal. B-Environ. 76 (2007) 241–247.
- [16] C. Thomas, Appl. Catal. B-Environ. 162 (2015) 454–462.
- [17] L. Strom, P.A. Carlsson, M. Skoglundh, H. Harelind, Appl. Catal. B-Environ. 181 (2016) 403–412.
- [18] P. Sazama, L. Capek, H. Drobna, Z. Sobalik, J. Dedecek, K. Arve, B. Wichterlova, J. Catal. 232 (2005) 302–317.
- [19] R. Brosius, K. Arve, M.H. Groothaert, J.A. Martens, J. Catal. 231 (2005) 344–353.
- [20] Y.B. Yu, H. He, X.L. Zhang, H. Deng, Catal. Sci. Technol. 4 (2014) 1239–1245.
- [21] K. Shimizu, K. Sawabe, A. Satsuma, Catal. Sci. Technol. 1 (2011) 331–341.
- [22] J. Shibata, K. Shimizu, S. Satokawa, A. Satsuma, T. Hattori, Phys. Chem. Chem. Phys. 5 (2003) 2154–2160.
- [23] U. Bentrup, M. Richter, R. Fricke, Appl. Catal. B-Environ. 55 (2005) 213–220.
- [24] K. Shimizu, A. Satsuma, T. Hattori, Appl. Catal. B-Environ. 25 (2000) 239–247.
- [25] F.C. Meunier, R. Ukropec, C. Stapleton, J.R.H. Ross, Appl. Catal. B-Environ. 30 (2001) 163–172.
- [26] A. Shichi, T. Hattori, A. Satsuma, Appl. Catal. B-Environ. 77 (2007) 92–99.
- [27] M. Richter, U. Bentrup, R. Eckelt, M. Schneider, M.M. Pohl, R. Fricke, Appl. Catal. B-Environ. 51 (2004) 261–274.
- [28] T. Miyadera, Appl. Catal. B-Environ. 2 (1993) 199–205.
- [29] K. Shimizu, J. Shibata, H. Yoshida, A. Satsuma, T. Hattori, Appl. Catal. B-Environ. 30 (2001) 151–162.
- [30] T. Chaieb, L. Delannoy, C. Louis, C. Thomas, Appl. Catal. B-Environ. 142 (2013) 780–784.
- [31] T. Chaieb, L. Delannoy, G. Costentin, C. Louis, S. Casale, R.L. Chanthery, Z.Y. Li, C. Thomas, Appl. Catal. B-Environ. 156 (2014) 192–201.
- [32] N.A. Sadokhina, A.F. Prokhorova, R.I. Kvon, I.S. Mashkovskii, G.O. Bragina, G.N. Baeva, V.I. Bukhtiyarov, A.Y. Stakheev, Kinet. Catal. 53 (2012) 107–116.
- [33] K. Shimizu, M. Tsuzuki, K. Kato, S. Yokota, K. Okumura, A. Satsuma, J. Phys. Chem. C 111 (2007) 950–959.
- [34] H. Deng, Y.B. Yu, F.D. Liu, J.Z. Ma, Y. Zhang, H. He, ACS Catal. 4 (2014) 2776–2784.
- [35] Y. Yan, Y.B. Yu, H. He, J.J. Zhao, J. Catal. 293 (2012) 13–26.
- [36] Y.B. Yu, J.J. Zhao, Y. Yan, X. Han, H. He, Appl. Catal. B-Environ. 136 (2013) 103–111.
- [37] X. She, M. Flytzani-Stephanopoulos, J. Catal. 237 (2006) 79–93.
- [38] H. Deng, Y.B. Yu, H. He, Chin. J. Catal. 36 (2015) 1312–1320.
- [39] H. Deng, Y.B. Yu, H. He, J. Phys. Chem. C 119 (2015) 3132–3142.
- [40] M. Digne, P. Sautet, P. Raybaud, P. Euzen, H. Toulhoat, J. Catal. 211 (2002) 1–5.
- [41] P.S. Kim, M.K. Kim, B.K. Cho, I.S. Nam, S.H. Oh, J. Catal. 301 (2013) 65–76.
- [42] B. Wichterlova, P. Sazama, J.P. Breen, R. Burch, C.J. Hill, L. Capek, Z. Sobalik, J. Catal. 235 (2005) 195–200.
- [43] G.D.-M.M. Boudart, Kinetics of Heterogeneous Catalytic Reactions, Princeton University Press, Princeton, NJ, 1984.
- [44] S. Tamm, L. Olsson, S. Fogel, P. Gabrielsson, M. Skoglundh, AIChE J. 59 (2013) 4325–4333.
- [45] B. Sawatmongkhon, A. Tsolakis, K. Theinnoi, A.P.E. York, P.J. Millington, R.R. Rajaram, Appl. Catal. B-Environ. 111 (2012) 165–177.
- [46] W.L. Johnson, G.B. Fisher, T.J. Toops, Catal. Today 184 (2012) 166–177.
- [47] S. Chansai, R. Burch, C. Hardacre, J. Breen, F. Meunier, J. Catal. 281 (2011) 98–105.
- [48] A.B. Mhadeshwar, B.H. Winkler, B. Eiteneer, D. Hancu, Appl. Catal. B-Environ. 89 (2009) 229–238.
- [49] D. Creaser, H. Kannisto, J. Sjoblom, H.H. Ingelsten, Appl. Catal. B-Environ. 90 (2009) 18–28.
- [50] J.R.H. Carucci, A. Kurman, H. Karhu, K. Arve, K. Eranen, J. Warna, T. Salmi, D.Y. Murzin, Chem. Eng. J. 154 (2009) 34–44.
- [51] K. Arve, J.R.H. Carucci, K. Eranen, A. Aho, D.Y. Murzin, Appl. Catal. B-Environ. 90 (2009) 603–612.
- [52] J.P. Breen, R. Burch, C. Hardacre, C.J. Hill, C. Rioche, J. Catal. 246 (2007) 1–9.
- [53] K. Arve, F. Klingstedt, K. Eranen, J. Warna, L.E. Lindfors, D.Y. Murzin, Chem. Eng. J. 107 (2005) 215–220.
- [54] K. Eranen, L.E. Lindfors, F. Klingstedt, D.Y. Murzin, J. Catal. 219 (2003) 25–40.
- [55] M. Hameda, Y. Kintaichi, H. Shimada, H. Hamada, J. Catal. 192 (2000) 137–148.
- [56] J.H. Li, R. Ke, W. Li, J.M. Hao, Catal. Today 139 (2008) 49–58.
- [57] F.C. Meunier, J.P. Breen, V. Zuzaniuk, M. Olsson, J.R.H. Ross, J. Catal. 187 (1999) 493–505.
- [58] Y.B. Yu, H. He, Q.C. Feng, H.W. Gao, X. Yang, Appl. Catal. B-Environ. 49 (2004) 159–171.
- [59] Y.B. Yu, X.P. Song, H. He, J. Catal. 271 (2010) 343–350.
- [60] M.I. Zaki, M.A. Hasan, L. Pasupulety, Langmuir 17 (2001) 768–774.
- [61] X.L. Zhang, H. He, H.W. Gao, Y.B. Yu, Spectrochim. Acta. A 71 (2008) 1446–1451.
- [62] K. Shimizu, J. Shibata, A. Satsuma, T. Hattori, Phys. Chem. Chem. Phys. 3 (2001) 880–884.
- [63] M. Digne, P. Sautet, P. Raybaud, P. Euzen, H. Toulhoat, J. Catal. 226 (2004) 54–68.
- [64] P. Nortier, P. Fourre, A.B.M. Saad, O. Saur, J.C. Lavalley, Appl. Catal. 61 (1990) 141–160.
- [65] J. Paier, C. Penschke, J. Sauer, Chem. Rev. 113 (2013) 3949–3985.
- [66] K. Shimizu, A. Satsuma, J. Phys. Chem. C 111 (2007) 2259–2264.